Available online at www.sciencedirect.com
SCIENCE DIRECT®
Applied Geochemistry 19 (2004) 917–936
Applied Geochemistry
www.elsevier.com/locate/apgeochem

Numerical simulation of CO_2 disposal by mineral trapping in deep aquifers

Tianfu Xu*, John A. Apps, Karsten Pruess

Earth Sciences Division, Lawrence Berkeley National Laboratory, University of California, Berkeley, CA 94720, USA

Received 3 April 2003; accepted 2 November 2003
Editorial handling by Y. Kharaka

Abstract

Carbon dioxide disposal into deep aquifers is a potential means whereby atmospheric emissions of greenhouse gases may be reduced. However, our knowledge of the geohydrology, geochemistry, geophysics, and geomechanics of CO_2 disposal must be refined if this technology is to be implemented safely, efficiently, and predictably. As a prelude to a fully coupled treatment of physical and chemical effects of CO_2 injection, the authors have analyzed the impact of CO_2 immobilization through carbonate mineral precipitation. Batch reaction modeling of the geochemical evolution of 3 different aquifer mineral compositions in the presence of CO_2 at high pressure were performed. The modeling considered the following important factors affecting CO_2 sequestration: (1) the kinetics of chemical interactions between the host rock minerals and the aqueous phase, (2) CO_2 solubility dependence on pressure, temperature and salinity of the system, and (3) redox processes that could be important in deep subsurface environments. The geochemical evolution under CO_2 injection conditions was evaluated. In addition, changes in porosity were monitored during the simulations. Results indicate that CO_2 sequestration by matrix minerals varies considerably with rock type. Under favorable conditions the amount of CO_2 that may be sequestered by precipitation of secondary carbonates is comparable with and can be larger than the effect of CO_2 dissolution in pore waters. The precipitation of ankerite and siderite is sensitive to the rate of reduction of Fe(III) mineral precursors such as goethite or glauconite. The accumulation of carbonates in the rock matrix leads to a considerable decrease in porosity. This in turn adversely affects permeability and fluid flow in the aquifer. The numerical experiments described here provide useful insight into sequestration mechanisms, and their controlling geochemical conditions and parameters.

1. Introduction

A reduction in the release rate of CO_2 to the atmosphere is considered as an essential first step in the control of global warming. One way of achieving this is to inject CO_2 into structural reservoirs in deep permeable geologic formations (Holloway, 1997). Such formations could include aquifers, oil and gas fields, and coal seams. Aquifers are the most abundant fluid reservoirs in the subsurface. The deepest aquifers in the United States commonly contain brackish or saline water. Aquifers with salinities exceeding 10,000 mg/l total dissolved solids (TDS) are excluded by the US Environmental Protection Agency as underground sources of drinking water. Hence, they are logical targets for the eventual disposal of CO_2. The feasibility of storing CO_2 in aquifers has been discussed in the technical literature over the last decade. These include an evaluation of the feasibility of CO_2 aquifer storage in The Netherlands (Lohuis, 1993) and in the Alberta Basin, Canada (Bachu et al., 1994, Law and Bachu, 1996, Gunter et al., 1993, 1996, 1997). Johnson et al. (2001) simulated the large scale injection of CO_2 currently being produced at Statoil's Sleipner facility in the Norwegian sector of the North Sea (Korbol and Kaddour, 1995). They analyzed the coupled processes and mechanisms that lead to

* Corresponding author. Fax: +1-510-486-5868.
E-mail address: tianfu_xu@url.gov (T. Xu).

0883-2927/$ - see front matter © 2003 Elsevier Ltd. All rights reserved.
doi:10.1016/j.apgeochem.2003.11.003

structural, solubility, and mineral trapping, and quantified the relative effectiveness of the distinct sequestration processes as a function of key reservoir properties. White et al. (2001) applied reactive chemical transport modeling to simulate mineral sequestration of CO_2 in saline reservoirs underlying the Colorado Plateau. McPherson and Lichtner (2001) used a mathematical sedimentary basin model, including multiphase flow of CO_2, groundwater, and brine, to evaluate resident times in possible aquifer storage sites and migration patterns and rates away from such sites in the Powder River Basin of Wyoming.

Carbon dioxide is retained in geologic formations in 3 ways (Hitchon, 1996). First, CO_2 can be trapped as a gas or supercritical fluid under a low-permeability caprock. This process, commonly referred to as hydrodynamic trapping, will be, in the short term, the most important method of retention. Second, CO_2 can dissolve into the groundwater, a process referred to as a solubility trapping. The latter increases the acidity of the groundwater and increases the solubilities of many minerals composing the host rock matrix. Third, CO_2 can react directly or indirectly with minerals in the geologic formation leading to the precipitation of secondary carbonate minerals. This so-called 'mineral trapping' (Bachu et al., 1994), is potentially attractive because it could immobilize CO_2 for very long periods of time. The dissolution of alkaline aluminosilicate minerals by CO_2 will also increase the concentration of soluble carbonates and bicarbonates in solution, thereby enhancing ''solubility trapping''.

The chemical reactions induced by CO_2 injection are described by Ortoleva et al. (1998). First, CO_2 dissolves in water to produce the weak carbonic acid:

$$CO_2(g) + H_2O = H_2CO_3 \quad (1)$$

This is followed by rapid dissociation of carbonic acid to form the bicarbonate ion:

$$H_2CO_3 = H^+ + HCO_3^- \quad (2)$$

The increased acidity induces dissolution of many of the primary host rock minerals, which in turn causes complexing of dissolved cations with the bicarbonate ion such as

$$Ca^{2+} + HCO_3^- = CaHCO_3^+ \quad (3)$$

The dissolved bicarbonate species react with divalent cations to precipitate carbonate minerals. Formation of Ca, Mg, and Fe(II) carbonates are expected to be the primary means by which CO_2 is immobilized (Gunter et al., 1997).

$$HCO_3^- + Ca^{2+} = CaCO_3(s) + H^+ \quad (4)$$

$$HCO_3^- + Mg^{2+} = MgCO_3(s) + H^+ \quad (5)$$

$$HCO_3^- + Fe^{2+} = FeCO_3(s) + H^+ \quad (6)$$

The authors surveyed major classes of rock-forming minerals whose alteration would lead to carbonate precipitation. Table 1 lists some major mineral classes and specifies the maximum quantity of CO_2 that could be sequestered by each mineral. The complete list is reported in Xu et al. (2000). The potential values are calculated by assuming complete alteration of the primary minerals. Actual sequestration capacity depends on the geochemical and physical conditions.

Table 1
Carbon dioxide sequestration potential of some major rock forming minerals

Mineral name	Mineral formula	Potential CO_2 fixed, kg/m^3 mineral
Plagioclase (anorthite)	$Ca[Al_2Si_2O_8]$	436.4
Olivine (forsterite-fayalite)	Mg_2SiO_4–Fe_2SiO_4	2014.7–1896.3
Pyroxene group-enstatite	$(Mg,Fe)_2Si_2O_6$	1404.2
Augite	$(Ca,Mg,Fe(II),Al)_2(Si,Al)_2O_6$	1306.3
Amphibole group-anthophyllite-cummingtonite	$(Mg,Fe(II),Fe(III),)_{5\text{-}7}Al_{0\text{-}2}[Si_{6\text{-}8}Al_{2\text{-}0}O_{22}](OH,)_2$	1169.5–1041.8
Common hornblende	$Ca_2Na_{0\text{-}1}(Mg,Fe(II))_{3\text{-}5}(Al,Fe(III))_{2\text{-}0}[Si_{6\text{-}8}Al_{2\text{-}0}O_{22}](O,OH)_2$	1000.4
Calcium amphiboles-tremolite	$Ca_2Na_{0\text{-}1}(Mg,Fe(II))_{3\text{-}5}(Al,Fe(III))_{2\text{-}0}[Si_{6\text{-}8}Al_{2\text{-}0}O_{22}](O,OH)_2$	1119.3
Mica group-glauconite	$(K,Na,Ca)_{1.2\text{-}2.0}(Fe(III),Al,Fe(II),Mg)_{4.0}[Si_{7\text{-}7.6}Al_{:\text{-}0.4}O_{20}](OH)_4.nH_2O$	61.97
Mica group-phlogopite	$K_2(Mg,Fe(II))_6[Si_6Al_{:2}O_{20}](OH)_4$	881.8
Mica group-biotite	$K_2(Mg,Fe(II))_{6\text{-}4}(Fe(III),Al)_{0\text{-}2}[Si_{6\text{-}5}Al_{:2\text{-}3}O_{20}](OH)_{4\text{-}2}$	671.0
Serpentine	$Mg_6Si_4O_{10}(OH)_8$	1232.7
Chlorite group	$(Mg,Al,Fe(II))_{12}[(Si,Al)_8O_{20}](OH)_{16}$	923.4
Clay minerals-illite	$K_{1\text{-}1.5}(Fe(III),Al,Fe(II),Mg)_{4.0}[Si_{7\text{-}6.5}Al_{:1\text{-}1.5}O_{20}](OH)_4$	78.42
Clay minerals-smectite	$(1/2Ca,Na)_{0.7}(Al,Mg,Fe)_4(Si,Al)_8O_{20}(OH)_4.nH_2O$	161.2

The potential for "mineral trapping" has prompted laboratory experimental studies in Europe (Pearce et al., 1996; Rochelle et al., 1996) and Canada (Gunter et al., 1997) to investigate this process. The European studies were carried out using reservoir sandstones and supercritical CO_2 at temperatures of 105 and 80 °C and CO_2 pressures of 90 and 200 bars, respectively, in autoclaves for periods of 1–8 months. The most notable observations were significant alteration of pre-existing calcite and dolomite, alteration of anhydrite with concomitant precipitation of calcite, and somewhat tenuous evidence for the corrosion of detrital feldspar and coupled precipitation of Na-smectite when in the presence of seawater.

The Canadian experiments were performed using samples from a glauconitic sandstone aquifer in the Alberta Sedimentary Basin, to validate results obtained with a batch geochemical model. The laboratory experiments were performed for one month at 105 °C at 90 bars CO_2 pressure to accelerate the reaction rate, because the kinetics of silicate reactions at room temperature are too slow to observe any significant CO_2 consumption in a reasonable length of time. The experimental results indicate that little CO_2 was trapped through reaction with aluminosilicate minerals on this time scale. The reactions observed involved the rapid dissolution of carbonate minerals. Geochemical modeling predicted that from 6 to 40 a were required for the experiments to reach equilibrium. Extending the model to the field, it was found by Gunter et al. (1997) that the CO_2 trapping reactions would take hundreds of years to complete after the formation water had equilibrated at the temperature of the aquifer (54 °C) at the proposed injection pressure (260 bar). However, they indicated that the reaction could be fast enough to form effective CO_2 mineral traps given the tens- to hundreds-of-thousands of years residence time of fluids in the deep aquifers.

Numerical modeling of geochemical processes is necessary to investigate long-term CO_2 injection in deep aquifers, because aluminosilicate mineral alteration is very slow under ambient deep-aquifer conditions and is not amenable to experimental study. Because the chemical composition of geologic formations varies widely, the authors present geochemical modeling analyses of the interaction of aqueous solutions under high CO_2 partial pressures with 3 different rock types.

The first rock is a glauconitic sandstone from the Alberta Sedimentary Basin, which had been evaluated previously by Gunter et al. (1997) as a potential host for CO_2 sequestration. In the present study, the mineral composition was modified to more closely reflect that observed, and Fe(III) reduction in glauconite was incorporated in the model. The second rock type evaluated, is a proxy for a sediment from the United States Gulf Coast (Apps, 1996). The mineralogy is similar to that commonly encountered in sedimentary basins. The third rock type is a dunite, an essentially monomineralic rock consisting of olivine. This rock is a mantle residue after depletion of basaltic magma, and occurs rarely at the earth's surface. However, it has a very large potential CO_2 sequestration capacity through mineral trapping.

The geochemical modeling under CO_2 injection conditions considered the following important factors affecting CO_2 sequestration: (1) the kinetics of chemical interactions between the host rock minerals and the aqueous phase, (2) CO_2 solubility dependence on pressure, temperature and salinity of the system, and (3) redox processes that could be important in deep subsurface environments. The CO_2 sequestration capacity of both aqueous and mineral phases was evaluated. Changes in porosity due to mineral dissolution and precipitation were also monitored.

2. Numerical modeling approach

2.1. Main features

The present simulations were carried out using the non-isothermal reactive geochemical transport code TOUGHREACT (Xu and Pruess, 1998, 2001). This code was developed by introducing reactive chemistry into the framework of the existing multi-phase fluid and heat flow code TOUGH2 (Pruess, 1991). The flow and transport in geologic media are based on space discretization by means of integral finite differences (Narasimhan and Witherspoon, 1976). An implicit time-weighting scheme is used for the individual components of the model consisting of flow, transport, and geochemical reaction. TOUGHREACT uses a sequential iteration approach, which solves the transport and the reaction equations separately. TOUGHREACT can also be used for batch geochemical modeling. Because only geochemical modeling features are used in the present simulations, discussion is restricted to those features of TOUGHREACT that relate to geochemistry.

The system of chemical reaction equations is solved by a Newton–Raphson iterative method similar to that of Parkhurst et al. (1980), Reed (1982), and Wolery (1992). Full details on numerical methods are given in Xu and Pruess (1998). The model can accommodate any number of chemical species present in liquid, gas and solid phases.

Local equilibrium is assumed to govern the distribution of aqueous chemical species. Because homogeneous reactions in the aqueous phase are almost instantaneous, they can be effectively considered at equilibrium. Coupled redox reactions are formulated in terms of dissolved O_2, where the chemical potential of the dissolved O_2 can be related to the oxidation state of the system

(Nordstrom and Muñoz, 1986; Wolery, 1992). In natural systems, many redox reactions that take place homogeneously within the aqueous phase are slow to achieve equilibrium, and therefore violate the local equilibrium assumption inherent in the current formulation of TOUGHREACT. This is consistent with observed discrepancies between the potentials estimated from different redox pairs (Stumm and Morgan, 1981). The validity of the local equilibrium assumption depends on the rate of transport relative to the rate of reaction. For long simulation times (more than 10 ka) with the present batch geochemical modeling, a chemical equilibrium assumption can be justified in most cases.

Mineral dissolution/precipitation can proceed subject either to local equilibrium or to kinetic conditions. The kinetic rate law used is given in Section 2.2. Thermodynamic and kinetic data are functions of temperature. The formulation of chemical equilibrium is similar to that by Parkhurst et al. (1980), Reed (1982), Yeh and Tripathi (1991), Wolery (1992), and Steefel and Lasaga (1994). The activity of aqueous species is equal to the product of the activity coefficient and molar concentration. Aqueous species activity coefficients with the exception of CO_2(aq) are calculated from the extended Debye–Hückel equation (Helgeson and Kirkham, 1974). The calculations of CO_2(aq) activity coefficient and CO_2(g) fugacity coefficient are presented in Section 2.3. Activities of pure mineral phases and H_2O are assumed to be unity. Mass conservation in the closed chemical system is written in terms of basis species. The species distribution must be governed by the total concentrations of the components.

2.2. Reaction rates

For kinetically-controlled mineral dissolution and precipitation, a general form of rate law (Lasaga, 1984; Steefel and Lasaga, 1994) is used

$$r_m = -\mathrm{sgn}\left[\log\left(\frac{Q_m}{K_m}\right)\right] k_m A_m \left|\left[\left(\frac{Q_m}{K_m}\right)^{\mu} - 1\right]\right|^n \tag{7}$$

where m is mineral index, r_m is the dissolution/precipitation rate (positive values indicate dissolution, and negative values precipitation), A_m is the specific reactive surface area per kg H_2O, k_m is the rate constant (mols per unit mineral surface area and unit time) which is temperature dependent, K_m is the equilibrium constant for the mineral-water reaction written for the destruction of one mole of mineral m, Q_m is ion activity product, the parameters μ and n are two positive numbers normally determined by experiment, and are usually, but not always, taken equal to unity (as in the present work). The expression "*sgn [log(Q/K)]*" ensures that the correct sign is enforced when the exponents μ and n are not equal to one. The temperature dependence of the reaction rate constant can be expressed reasonably well via an Arrhenius equation (Lasaga, 1984; Steefel and Lasaga, 1994). Since many rate constants are reported at 25 °C, it is convenient to approximate rate constant dependency as a function of temperature, thus

$$k = k_{25}\exp\left[\frac{-E_a}{R}\left(\frac{1}{T} - \frac{1}{298.15}\right)\right] \tag{8}$$

where E_a is the activation energy, k_{25} is the rate constant at 25 °C, R is gas constant, and T is absolute temperature.

2.3. CO_2 solubility

Gaseous and aqueous CO_2 are assumed to be in equilibrium, thus, $CO_2(g) = CO_2(aq)$. According to the mass-action law, we have

$$K\Gamma P = \gamma C \tag{9}$$

where K is the equilibrium constant, Γ is the gaseous CO_2 fugacity coefficient, P is the partial pressure (bar), γ is the aqueous CO_2 activity coefficient, and C is the aqueous concentration (mol/kg H_2O).

The equilibrium constant K at different temperatures can be derived from the following expression:

$$\log K = b_1 \ln T + b_2 + b_3 T + \frac{b_4}{T} + \frac{b_5}{T^2} \tag{10}$$

where the values of the coefficients b_1, b_2, b_3, b_4 and b_5 are obtained from the log$K$ values at 0, 25, 60, 100, 150, 200, 250, and 300 °C. Based on log$K$ values at these temperatures given in EQ3/6 geochemical database (Wolery, 1992), the following values of the coefficients were obtained: $b_1 = 65.48$, $b_2 = -425.5$, $b_3 = -0.05301$, $b_4 = 24010$, $b_5 = -1.22\times10^6$. Pressure dependence of K values was not considered.

At low pressures (in the range of atmospheric pressure), the gaseous species are assumed to behave as an ideal mixture, and the fugacity coefficient is assumed equal to unity. At higher temperatures and pressures characteristic of CO_2 deep aquifer injection and boiling conditions in hydrothermal systems, the assumption of ideal gas and ideal mixing behavior is not valid, and the fugacity coefficients should be corrected according to temperatures and pressures of the study system (Spycher and Reed, 1988). For the present H_2O–CO_2 mixture conditions, it is assumed that H_2O and CO_2 are real gases, but form an ideal mixture. According to Spycher and Reed (1988), the fugacity coefficients can be calculated from

$$\ln\Gamma = \left(\frac{a}{T^2} + \frac{b}{T} + c\right)P + \left(\frac{\mathrm{d}}{T^2} + \frac{e}{T} + f\right)\frac{P^2}{2} \tag{11}$$

where P is the total gas pressure (vapor and CO_2), T is absolute temperature, and a, b, c, d, e, and f are constants fitted from experimental data. For P–T

ranges, 50–350 °C, up to 500 bars, the fitted constants have the following values: $a=-1430.87$, $b=3.598$, $c=-2.27376\times10^{-3}$, $d=3.47644$, $e=-1.04247\times10^{-2}$, and $f=8.46271\times10^{-6}$. Examples of equilibrium calculations between aqueous and gas phases show that ideal mixing of real gases is an adequate approximation in the above-mentioned P–T ranges (Spycher and Reed, 1988).

For low ionic strength solution, CO_2(aq) activity coefficient γ can be assumed equal to one. For high ionic strength NaCl solution, γ should be corrected to account for the salting out effect. Here an activity coefficient expression of Drummond (1981) is used for the neutral CO_2(aq) species:

$$\ln\gamma = \left(C + FT + \frac{G}{T}\right)I - (E + HT)\left(\frac{I}{I+1}\right) \tag{12}$$

where T is the absolute temperature, I is ionic strength (or NaCl molality), C, F, G, E, and H are constants ($C=-1.0312$, $F=0.0012806$, $G=255.9$, $E=0.4445$, and $H=-0.001606$). This expression was previously used in geochemical modeling codes EQ3/6 (Wolery, 1992). The ionic strength I is defined by

$$I = \frac{1}{2}\sum_i c_i z_i^2 \tag{13}$$

where the summation is over all aqueous species, and c_i and z_i are concentration (mol/kg H_2O) and electrical charge of species i.

2.4. Thermodynamic data

The quality and accuracy of geochemical modeling is enhanced through the use of internally consistent and critically evaluated thermodynamic data derived from a comprehensive review of the published literature. The primary source for equilibrium constants for aqueous species and minerals used in this study originated with the EQ3/6 V7.2b database (Wolery, 1992). However, many substitutions and changes were incorporated in response to more recent published revisions in the thermodynamic properties of several rock forming minerals and aqueous species. Among these were revisions to the feldspars by Arnorsson and Stefansson (1999), several clay minerals by Kulik and Aja (1997), and dawsonite (Ferrante et al., 1976). In addition, a comprehensive revision to the properties of silica polymorphs and SiO_2(aq) was initiated as a result of a recent refinement by Rimstidt (1997) of the low temperature aqueous solubility of quartz. Revised thermodynamic properties of relevant aqueous species based on the Helgeson–Kirkham–Flowers (HKF) equation of state (Shock et al., 1997), including Al species were also incorporated. Changes in the properties of SiO_2(aq) and AlO_2^- necessitated recomputation of the solubility products for all minerals containing silica or alumina components, whose thermodynamic properties were based on calorimetric measurements. The following C-bearing aqueous species are also incorporated in the present modeling: CO_2(aq), HCO_3^- CO_3^{2-}, CH_4(aq), $FeHCO_3^+$, $NaHCO_3$(aq), $CaHCO_3^+$, $MgHCO_3^+$, $CaCO_3$(aq), $MgCO_3$(aq), $FeCO_3$(aq), acetic acid, and acetate.

To ensure consistency with unmodified equilibrium constants in the EQ3/6 V7.2b database, previously generated from thermodynamic data using SUPCRT92 (Johnson et al., 1992), all revised thermodynamic data were incorporated in the SUPCRT92 database and new equilibrium constants similarly generated.

In addition to the changes noted above, the thermodynamic properties of several other phases were estimated and their solubility products incorporated to improve model versimilitude, including glauconite, oligoclase, ankerite, and type II kerogen. Brief descriptions regarding the methods used to calculate their properties follow.

2.4.1. Glauconite

Complete documentation for the calculation of glauconite thermodynamic properties are given in Xu et al. (2000). A representative chemical composition was chosen, which falls close to the center of a ternary compositional field for glauconite, defined by Koster (1982) and Bailey (1986). The dissolution reaction of glauconite was written as follows:

$$\begin{aligned} &K_{1.5}\left(Mg_{0.5}Fe^{III}_{2.5}Fe^{II}_{0}{}_{.5}Al_{0.5}\right)\,[Al_{0.5}Si_{7.5}O_{20}](OH)_4 + 14H^+ \\ &= 1.5K^+ + 2.5Fe^{3+} + 0.5Fe^{2+} + Mg^{2+} \\ &\quad + 1.0Al^{3+} + 7.5SiO_2(aq) + 9H_2O \end{aligned} \tag{14}$$

It was used to calculate the Gibbs free energy of formation of glauconite, $G^o_{f,\ \mathrm{Tr,Pr}}$(glauconite), using the EQ3/6, assuming coexistence at equilibrium with a representative suite of primary and secondary minerals commonly observed to coexist with glauconite under diagenetic conditions. The resulting value was independently checked using the oxide/hydroxide component summation method of Chermak and Rimstidt (1989), and agreement obtained to within 0.5%. Molar volume was calculated from crystallographic data, and entropy and heat capacity were calculated according to methods suggested by Helgeson et al. (1978). Solubility product data was computed with the aid of SUPCRT92.

2.4.2. Oligoclase

Detrital plagioclase in most sediments is typically oligoclase in composition. Calculation of the thermodynamic properties of oligoclase is facilitated by the availability of calorimetric data in the form of the enthalpies of solution of high structural state plagioclases (Newton et al., 1980), from which the cited authors computed expressions for the excess enthalpy of mixing, ΔH^{ex}, and the Gibbs free energy of mixing, ΔG^{mix}, respectively, for the anorthite ($CaAl_2Si_2O_8$)–albite ($NaAlSi_3O_8$) series.

For convenience, and because it closely represents the composition of oligoclase actually found in many arkosic and characteristic sandstones, the following stoichiometry was chosen for oligoclase: $CaNa_4Al_6Si_{14}O_{40}$. Calculation of $\Delta G^o_{f,\ \mathrm{Tr,Pr}}$,(oligoclase) proceeded in two steps; (1) calculation of $\Delta G^o_{f,\ \mathrm{Tr,Pr}}$ of the physical mixture of anorthite and high albite corresponding to the stoichiometry of oligoclase, and (2) Incorporation of the correction for the Gibbs free energy of mixing, ΔG^{mix}, according to the data of Newton et al. (1980). The remaining properties, V°, S°, and C_P and the solubility products were calculated as described for glauconite, above. Complete details of the calculations are given in Xu et al. (2000).

2.4.3. Ankerite

Ankerite ($Ca(Fe,Mg)(CO_3)_2$) occurs in Gulf Coast sediments at depths corresponding to those where petroleum maturation occurs, with concomitant increases in CO_2 partial pressures (Franks and Forester, 1984; Gouze and Coudrain-Ribstein, 2002). It has also been observed to form in a natural gas reservoir contaminated with substantial quantities of magmatic CO_2 (Watson et al., 2002). Hence, it is important that this phase can be considered as a potential product mineral in geochemical simulations of CO_2 sequestration. Despite its relative importance, however, the thermodynamic properties of ankerite are incompletely known. A binary solution, $Ca(Fe_xMg_{1-x})(CO_3)_2$, where $0 < x < 0.7$ is observed in nature (Essene, 1983), but end-member ankerite, $CaFe(CO_3)_2$, has never been observed, its place being taken by coexisting siderite and calcite (Goldsmith, 1983; Chai and Navrotsky, 1996). The thermodynamic properties of the most Fe-rich member of the ankerite solid solution, $Ca(Fe_{0.7}Mg_{0.3})(CO_3)_2$ were calculated. An ideal solid solution is assumed between dolomite and end-member ankerite. The lattice energies reported by Chai and Navrotsky (1996) for the system calcite-siderite-magnesite together with the corresponding ΔH^o_f for calcite, magnesite and siderite from the SUPCRT92 database (Johnson et al., 1992) were used to determine the enthalpy of formation, $\Delta H^o_{f,298.15}$. The entropy, $S^o_{f,298.15}$ was calculated from the end member values reported by Holland and Powell (1998), a small correction being applied to ensure consistency with dolomite data in the SUPCRT92 database. The Maier–Kelley heat capacity coefficients were calculated from the corresponding coefficients for dolomite, siderite and magnesite in the SUPCRT92 database, again assuming ideal mixing. Appropriate dissolution constants for the reaction:

$$Ca(Fe_{0.7}Mg_{0.3})(CO_3)_2 + 2H^+ = Ca^{2+} + 0.7Fe^{2+} + 0.3Mg^{2+} + 2HCO_3^- \quad (15)$$

were calculated with the aid of SUPCRT92 and incorporated in the TOUGHREACT database.

2.4.4. Type II Kerogen

Kerogen plays an extremely important role in the diagenesis of sediments, and is an essential constituent in any geochemical simulation of such a process. Its representation is, however, a particular challenge. For while an extensive descriptive literature describes its occurrence and maturation, little has been done to describe the maturation process that would be quantitatively suitable for incorporation in any thermochemical simulation. As a guide in developing a preliminary model, the authors referred to Behar and Vandenbroucke (1986) who have attempted to describe quantitatively the composition of the various kerogen types, and their degree of maturation in terms of the distribution of linear and polycyclic alkanes, aromatic hydrocarbons, and attached oxygenated, thio and amino functional groups.

It is assumed that Type II kerogen continuously alters from an early stage of diagenesis (stage a) to the onset of catagenesis (stage b, the incipient formation of oil), (Behar and Vandenbroucke, 1986) as a single process. It does not account for differential rates of decarboxylation by different oxygenated functional groups. This is a simplification of the progressive loss of functional groups with time and temperature elevation during progressive burial, but suffices for a preliminary evaluation. It is also assumed that there is only partial loss of oxygenated functional groups, which is consistent with the bulk changes in H/C and O/C atomic ratios. The decomposition of thio, amino and amide groups are ignored. A further simplification was to assume that the functional groups, whether attached to aliphatic or aromatic ligands, were equivalent. The depletion of O is primarily associated with loss of the hydroxy, acid, ester and amide groups. For initial modeling purposes, only the first 3 groups are considered, and these are approximated to the ratio of 18:5:6 to avoid fractional stoichiometry in thermochemical calculations.

Intermediate products of decarboxylation are primarily aliphatic acids, which are commonly encountered in oil field waters in concentrations up to 8000 mg/l, (see Helgeson et al., 1993 for a review). Of these acids, acetic acid is dominant. It is therefore assumed that depletion of the oxygenated functional groups can be represented stoichiometrically by the following reactions. For alcohols:

$$\mathbf{R}\text{-}CH_2OH = \mathbf{R}\text{-}H + 0.5\ CH_3COOH \quad (16)$$

or by subtracting R and H from both sides:

$$\text{-}CHOH = 0.5\ CH_3COOH \quad (17)$$

Similarly, for acids and esters:

$$\text{-}CHCOOH + H_2O = CH_3COOH + 0.5\ O_2(g) \quad (18)$$

$$\text{-CHCOOCH}_2\text{CH}_3 + 0.5\ \text{O}_2(\text{g}) + \text{H}_2\text{O} = 2\ \text{CH}_3\text{COOH} \quad (19)$$

Summing reactions (17), (18) and (19) in the ratio of 18:5:6, we get

$$(\text{-CHOH})_{18}(\text{-CHCOOH})_5(\text{-CHCOOCH}_2\text{CH}_3)_6 + 11\ \text{H}_2\text{O} + 0.5\ \text{O}_2(\text{g}) = 26\text{CH}_3\text{COOH(aq)} \quad (20)$$

The stoichiometry of the above reactions constrains the loss of H, and hence the H/C ratio of the residual partially deoxygenated kerogen. This in turn constrains the ratio of alkanes to aromatics. It is assumed that the hydrocarbon component consists of linear alkanes with an average chain length of 21 C ($C_{21}H_{44}$), cycloalkanes with an average of 3 linked closed cycles ($C_{14}H_{24}$) and aromatics with 3 rings, e.g. anthracene ($C_{14}H_{10}$). Given that the residual kerogen has a bulk composition of $H_{25.74}C_{21}$, and assuming the cyclo-alkane content to be 2.94 C, the molar fractions of alkane: cycloalkane:aromatic is calculated to be 0.2689:0.14000:0.5911. These ratios were used in distributing the oxygenated functional groups over the alkane, cycloalkane and aromatic components of the kerogen.

In computing the thermodynamic properties of the attached oxygenated functional groups, the molal properties (ΔG°_f, ΔH°_f, S°, and the Maier–Kelley heat capacity coefficients, a, b, c) of functional group components were taken from Helgeson et al. (1998) and Richard and Helgeson (1998). The properties of the oxygenated functional groups were summed and appropriate dissociation equilibria for reaction (20) calculated with the aid of SUPCRT92 (Johnson et al., 1992).

Evidence that dissolved aliphatic acids are in metastable redox equilibrium with carbonate species in oilfield brines is quite strong (Helgeson et al., 1993). Acetic acid and acetate ion are therefore assumed to be in redox equilibrium with bicarbonate species, thus:

$$\text{CH}_3\text{COOH(aq)} + 2\text{O}_2(\text{g}) = 2\text{HCO}_3^- + 2\text{H}^+ \quad (21)$$

Dissociation constant data for acetic acid and acetate oxidation were calculated using SUPCRT92 with the SPRONS96.DAT database. Complexation of acetate with metal cations, e.g. Ca^{2+} and Al^{3+}, were not incorporated in the present model, to avoid uneccessary complexity.

As noted above, acetic acid is the dominant aliphatic acid in oil field brines, but it is not clear whether aliphatic acids are in thermodynamic equilibrium under field conditions (Helgeson et al., 1993; Bell and Palmer, 1994). Because of this uncertainty, and because the concentrations of aliphatic acids other than acetic acid are relatively minor, only acetic acid and acetate were incorporated in the model.

2.5. Kinetic data

Mineral dissolution and precipitation rates are a product of the kinetic rate constant and reactive surface area [Eq. (7)], the magnitudes of which are highly uncertain and cover a wide range of values. The temperature-dependent kinetic rate constants are calculated from Eq. (8), and the required parameters, kinetic constant at 25 °C (k_{25}) and activation energy (E_a), are given in Table 2. Some kinetic parameters were taken directly from published scientific literature. The references are listed in the fourth column of Table 2. Others were set to the minerals with known kinetic properties. The evolution of surface area in natural geologic media is very complex, especially for multi-mineralic systems, and is not quantitatively understood at present. Mineral reactive surface areas (last column of Table 2) were taken from Sonnenthal and Spycher (2001), which were calculated using the geometric area of a cubic array of truncated spheres that make up the framework of the rock. A reactive surface area calculated from grain size may be a poor estimate of the hydrologically accessible mineral surface area. A sensitivity analysis regarding reaction rates can give some understanding of its impact on the overall geochemical behavior of the system (Section 4.4).

The precipitation of possible secondary minerals is represented using the same kinetic expression as that for dissolution. However, several aspects regarding precipitation are different, including nucleation, crystal growth and Ostwald ripening processes, as well as the calculation of the reactive surface area (Steefel and van Capellen, 1990).

3. Problem setup

3.1. Glauconitic sandstone

The first mineral assemblage is representative of a glauconitic sandstone aquifer from the Alberta Sedimentary Basin, which had been studied previously by Gunter et al. (1997). The glauconitic sandstone is a medium- to fine-grained litharenite. The average mineral composition is 87% quartz, 2% K-feldspar, 1% plagioclase, 5% glauconite, 2% kaolinite, 1% calcite, 1% dolomite, and 1% siderite. The average porosity is 12%. Gunter et al. (1997) modeled water–rock reactions driven by the formation of carbonic acid when CO_2 is injected into deep aquifers using PATHARC.94 (Perkins and Gunter, 1995). In their simulations, the CO_2 injection pressure was set at 260 bar. Annite was used as a proxy for glauconite. Plagioclase was simulated by using discrete fractions of end member components, anorthite and albite.

The use of annite as a substitute for glauconite overestimates the availability of Fe^{2+}, the amount of siderite

Table 2
List of kinetic rate parameters for minerals considered in the 3 types of rock

Mineral	k_{25} (mols $m^{-2}s^{-1}$)	E_a (KJ/mol)	Reference	Surface area (g/cm)
quartz	1.2589×10^{-14}	87.50	Tester et al. (1994)	98
K-feldspar	1.00×10^{-12}	67.83	Blum and Stillings (1995)	98
kaolinite	1.00×10^{-13}	62.76	Nagy (1995)	100
calcite	1.60×10^{-9}	41.87	Svensson and Dreybrodt (1992)	98
dolomite	0.60×10^{-9}	41.87	assumed based on calcite	98
siderite	0.60×10^{-9}	41.87	assumed based on calcite	98
illite	1.00×10^{-14}	58.62	Knauss and Wolery (1989)	1516
glauconite	1.00×10^{-14}	58.62	set to illite	1516
Kerogen-O	1.00×10^{-13}	0.0	assigned based on kaolinite	100
oligoclase	1.00×10^{-12}	67.83	set to K-feldspar	100
albite-low	1.00×10^{-12}	67.83	Blum and Stillings (1995)	98
Na-smectite	1.00×10^{-14}	58.62	set to illite	1516
Ca-smectite	1.00×10^{-14}	58.62	set to illite	1516
pyrite	4.00×10^{-13}	0.0	Ague and Brimhall (1989)	129
forsterite	1.00×10^{-13}	62.76	set to kaolinite	98
fayalite	1.00×10^{-13}	62.76	set to kaolinite	98
magnesite	0.60×10^{-9}	41.87	assumed based on calcite	98
amorphous silica	1.00×10^{-13}	62.76	set to kaolinite	98
goethite	1.00×10^{-14}	58.62	set to illite	98
dawsonite	1.00×10^{-12}	67.83	set to K-feldspar	98
ankerite	0.60×10^{-9}	41.87	assumed based on calcite	98
clinochlore-14A	1.00×10^{-14}	58.62	set to illite	98
daphnite-14A	1.00×10^{-14}	58.62	set to illite	98

($FeCO_3$) precipitation, and hence the degree of CO_2 sequestration. In the present study, the mineral assemblage was modified to more closely reflect that expected in a glauconitic sandstone. Thus, the authors estimated a representative glauconite chemical composition and thermodynamic properties from descriptions of the mineralogical compositions of glauconite and its paragenesis (see Section 2.4). Oligoclase was also incorprated as a solid solution of plagioclase, and the thermodynamic properties of oligoclase were calculated from calorimetric studies of plagioclase solid solutions. Rather than using muscovite as a proxy for illite, it was assumed that illite was actually present as a primary mineral. Finally, it was assumed that organic matter, represented by type II kerogen designated kerogen-O, was present in the glauconitic sandstone. The initial mineral abundances used in the present modeling (Table 3), are based on the previous work (Hitchon, 1996), but with the addition of a 2.64% volume fraction of organic matter. Goethite (FeOOH), ankerite and dawsonite [$NaAlCO_3(OH)_2$] were also added as secondary minerals. Goethite precipitation competes with siderite for Fe, which could reduce the amount of CO_2 sequestration. The carbonate bearing mineral dawsonite could also precipitate due to high pressure CO_2 and dissolution of alumino-silicate minerals. In addition, the authors accounted for redox sensitive couples such as Fe^{3+}/Fe^{2+}, $CO_2(aq)/CH_4(aq)$, $H_2O(aq)/H_2(aq)$, and SO_4^{2-}/HS^-, which are very important in the geochemical evolution of sedimentary basins.

3.2. Gulf Coast sediments

A proxy for a sediment from the United States Gulf Coast modified from that originally presented by Apps (1996) was used. This mineralogy is similar to that commonly encountered in sedimentary basins. Apps (1996) presented a batch geochemical simulation of the evolution of Gulf Coast sediments as a basis for interpreting the chemical processes relating to the deep injection disposal of hazardous and industrial wastes. Gulf Coast Mesozoic and Tertiary sediments are characterized by rapid burial and incorporation of significant amounts of organic matter, especially in shales. The maturation of the organic matter into petroleum and natural gas, and its migration into numerous structural traps is a characteristic of these sediments. Therefore, a simulation should incorporate a representation of maturing organic matter. Another feature of relevance is the entrapment of evaporite salt beds during sedimentary accumulation. Over time, the salt has migrated into diapirs, modifying sedimentary accumulation during concurrent sedimentation and subsidence, and generating salt domes, which commonly trap oil and gas accumulations along their flanks. The salt domes are known to dissolve partially into ground-

Table 3
List of initial mineral volume fractions and potential secondary mineral phases for the glauconitic sandstone

Mineral	Chemical composition	Volume (%)
Primary		
quartz	SiO_2	71.28
K-feldspar	$KalSi_3O_8$	1.76
kaolinite	$Al_2Si_2O_5(OH)_4$	1.76
calcite	$CaCO_3$	0.88
dolomite	$CaMg(CO_3)_2$	0.88
siderite	$FeCO_3$	0.88
illite	$K_{0.6}Mg_{0.25}Al_{1.8}(Al_{0.5}Si_{3.5}O_{10})(OH)_2$	2.64
glauconite	$K_{1.5}Mg_{0.5}Fe_{2.5}Fe_{0.5}AlSi_{7.5}O_{20}(OH)_2$	4.4
kerogen-O	$C_{52}H_{82}O_{40}$	2.64
oligoclase	$CaNa_4Al_6Si_{14}O_{40}$	0.88
porosity	–	12
total	–	100
Secondary		
albite-low	$NaAlSi_3O_8$	0.0
Na-smectite	$Na_{0.290}Mg_{0.26}Al_{1.77}Si_{3.97}O_{10}(OH)_2$	0.0
Ca-smectite	$Ca_{0.145}Mg_{0.26}Al_{1.77}Si_{3.97}O_{10}(OH)_2$	0.0
goethite	FeOOH	0.0
dawsonite	$NaAlCO_3(OH)_2$	0.0

waters, elevating the salinity. Thus a simulation should also include an initial concentration of dissolved NaCl.

The initial mineral abundances used in the present batch geochemical modeling (Table 4), are refined from the previous batch geochemical modeling study by Xu et al. (2000). The specification of formation mineralogy is determined in part by the availability of data. Most studies related to the Tertiary Gulf Coast sediments are concentrated in the state of Texas. The principal reservoir-quality sandstones within that region are respectively, the Frio, the Vicksberg and the Wilcox formations, all of which are found within the Lower Tertiary. Of the 3 formations, the Frio was chosen as a representative candidate for the sequestration of supercritical CO_2. It is the shallowest of the 3 formations, but over much of its areal extent, it is located at depths between 1520 and 6100 m, sufficient to ensure adequate CO_2 densities for effective storage.

Loucks et al. (1984) used the sandstone classification of Folk (1968) to describe sandstone reservoirs in the Lower Tertiary Gulf Coast sediments of Texas. According to these authors, the Frio shows the greatest variation in mineral composition ranging from poorly sorted fine-grained feldspathic litharenites to lithic arkoses to fine-grained lithic arkoses and sub-arkoses. For the purposes of this study, the approximate mean composition of the Frio in the Middle Texas region of the Gulf Coast was chosen. This composition is representative of a quartzose lithic arkose with 56% quartz (by weight), 28% feldspar and 16% lithic fragments. According to Loucks et al. (1984), the lithic fragments in the Frio formation of this region are predominantly volcanic fragments, although significant percentages of metamorphic rocks are present. Carbonate rock fragments are also present, but are less common than along the lower Texas Gulf Coast. The volcanic rocks of the lower Texas Gulf Coast are dominantly rhyolites and trachytes, which have been silicified or altered to chlorite. Those volcanic rocks of the middle Texas Gulf Coast are apparently of similar composition and provenance, but less abundant. The carbonate fragments were apparently locally derived from adjacent landmass caliche soils. Neither the provenance nor the character of the metamorphic rocks is described.

For the purposes of simulation, the actual mineral composition of the sandstone is required. This necessitates knowing the fractions of plagioclases and alkali feldspars making up the feldspar component, and the mineralogy of the lithic fragments. Land (1984) reports that 1634 electron probe point counts on 29 Frio formation rocks indicate that about 30 wt.% of the original feldspar was K-feldspar and the remainder was plagioclase having an average anorthite content of 20 wt.%. The concentration of K feldspar is therefore somewhat higher than specified by Tempel and Harrison (2000) who modeled a feldspathic litharenite belonging to the underlying Wilcox Formation comprising, which comprised 25.8 wt.% plagioclase with content of 25 wt.% anorthite and 5 wt.% K-feldspar. The composition of the lithic fragments has been described only in a qualitative sense, and therefore, the actual mineral composition can only be surmised. Furthermore, secondary minerals (calcite, clay minerals, and Fe oxides) are not included in published lithological classifications. Therefore, the inclusion of these phases must also necessarily be determined subjectively.

The representative mineral composition of a quartzose lithic arkose from the Middle Texas area of the Frio formation given in Table 4 was assigned abundances using the following arguments: (1) Two wt.% of calcite was added to reflect the presence of fragments of caliche present in the Frio (Loucks et al., 1984). (2) The observed presence of chlorite in lithic fragments of volcanic rock (Loucks et al., 1984) is represented by 3 wt.% clinochlore and 2 wt.% daphnite, representing the Mg and Fe(II) end members, respectively of a 14 A chlorite solid solution. (The present version of TOUGHREACT does not presently have the capability of incorporating solid solutions.) (3) A small amount of hematite (1 wt.%) was added to take into account the presence of Fe(III) staining. The chosen concentration is consistent with independent modeling by Tempel and Harrison (2000). (4) Organic Matter, as a Type II kerogen, designated kerogen-O, is arbitrarily assigned an abundance of 1 wt.%. The shale confining beds of the Gulf Coast,

Table 4
List of initial mineral volume fractions and possible secondary mineral phases for Gulf Coast sediments (based on Apps, 1996)

Mineral	Chemical composition	Wt.%	Vol.%
Primary			
quartz	SiO_2	56	49.7466
kaolinite	$Al_2Si_2O_5(OH)_4$	2	1.8135
calcite	$CaCO_3$	2	1.7361
illite	$K_{0.6}Mg_{0.25}Al_{1.8}(Al_{0.5}Si_{3.5}O_{10})(OH)_2$	1	0.8586
kerogen-O	CH_2O	1	2.6136
oligoclase	$CaNa_4Al_6Si_{14}O_{40}$	20	17.8155
K-feldspar	$KAlSi_3O_8$	8	7.3611
Na-smectite	$Ca_{0.145}Mg_{0.26}Al_{1.77}Si_{3.97}O_{10}(OH)_2$	4	3.5073
Clinochlore-14A	$Mg_5Al_2Si_3O_{10}(OH)_8$	3	2.6793
Daphnite-14A	$Fe_5Al_2Si_3O_{10}(OH)_8$	2	1.4211
hematite	Fe_3O_3	1	0.4473
porosity	–		10
total	–		100
Secondary			
albite-low	$NaAlSi_3O_8$		0.0
Dolomite	$CaMg_{0.3}Fe_{0.7}(CO_3)_2$		0.0
Siderite	$FeCO_3$		0.0
Ca-smectite	$Na_{0.290}Mg_{0.26}Al_{1.77}Si_{3.97}O_{10}(OH)_2$		0.0
pyrite	FeS_2		0.0
ankerite	$CaMg(CO_3)_2$		0.0
dawsonite	$NaAlCO_3(OH)_2$		0.0

representing a substantially larger mass than the enclosed aquifers, are estimated to contain about 1 wt.% organic C (Hunt, 1972), as cited by Franks and Forester (1984). However, this abundance is probably much higher than is found in the matrix of contiguous sandstones. Given that the adjacent shales are probably the primary source of chemical constituents of secondary minerals in the sandstone aquifers, and that certain compromises are needed with preliminary model approximations, it is useful to assume that the modified sandstone aquifer contains about 1 wt.% of Type II kerogen. (5) The concentrations of clay minerals, smectite, illite and kaolinite were arbitrarily assigned abundances of 4, 1 and 2 wt.% respectively and assigned as the residue of the mineral contribution by lithic fragments. The compositions of smectite and illite are those representative of illite/smectite (I/S) clays, typical of Gulf Coast sediments. The smectite could be of detrital or diagenetic origin, and could be separated from the lithic fragments, or included as an alteration product within the fragments.

3.3. Dunite

The third rock type investigated was dunite, an monomineralic rock consisting essentially of olivine. This rock is a mantle residue after depletion of basaltic magma, and occurs rarely at the earth's surface. However, it has a very large CO_2 sequestration capacity (see Table 1), and was chosen to be illustrative of the extreme limits possible for CO_2 sequestration by mineral trapping. Olivine is a binary solid solution of the pure end-member minerals, forsterite (Mg_2SiO_4) and fayalite (Fe_2SiO_4). The volume ratio of these end member components in typical olivine is about 9:1. The initial mineral abundances used in the simulations are presented in Table 5. The porosity of dunite is commonly small, and an initial porosity of 0.05 was assumed. The possible secondary mineral phases under CO_2 injection are also listed in Table 5.

Simulations for each rock type were performed under a CO_2 injection pressure of 260 bar. This pressure is based on the assumption that the aquifer is 1500 m deep, and can sustain this CO_2 injection pressure (Gunter et al., 1997). The CO_2 gas pressure is assumed to be in equilibrium with the solution at all times. Thus, the CO_2 gas is treated as an exterior boundary condition with a constant pressure. The solubility of CO_2 in the aqueous phase depends on pressure, temperature, and salinity (Section 2.3). The geochemical simulations consider 1 m^3 of water-saturated medium. The initial conditions used in the simulation are a pure 1.0 M solution of NaCl reacting with the primary minerals at a temperature of 54 °C for the first rock and 80 °C for second and third rocks, a pH of 7 and an Eh of −0.1 V for all 3 rocks.

Table 5
List of initial mineral volume fractions and possible secondary mineral phases for dunite

Mineral	Chemical composition	Volume (%)
Primary		
forsterite	Mg_2SiO_4	85.5
fayalite	Fe_2SiO_4	9.5
porosity	–	5.0
total	–	100
Secondary		
Magnetite	Fe_3O_4	0.0
Magnesite	$MgCO_3$	0.0
Siderite	$FeCO_3$	0.0
Talc	$Mg_3Si_4O_{10}(OH)_2$	0.0
Amorphous silica	SiO_2	0.0
iron	Fe	0.0

4. Results and discussion

4.1. Mineral alteration

With the imposition of a constant CO_2 pressure of 260 bar, an abrupt change of water composition occurs. The pH falls to about 5 and Eh rises to about 0.1 V in each of the 3 rock types. Both parameters are strongly buffered by the CO_2 gas pressure.

For glauconitic sandstone, mineral abundances after 100 ka are presented in Fig. 1. Glauconite (Fig. 1a) dissolves until disappeared after approximately 20 ka. Kerogen-O dissolve at a constant rate. Oligoclase, kaolinite and calcite dissolve rapidly (disappeared after 1 ka). Illite and K-feldspar (Fig. 1a) precipitates. No smectite is formed. Carbonate minerals dolomite and dawsonite precipitate (Fig. 1b) to a limited extent. Siderite and ankerite precipitation is significantly greater, because of greater availability of carbonate and more rapid glauconite dissolution. Goethite (Fig. 1a) initially precipitates and later dissolves, after the disappearance of glauconite, for supplying the Fe needed for siderite and ankerite precipitation.

For Gulf Coast sediments, clinochlore-14A and daphnite-14A dissolution (Fig. 2 a) occurs steadily with a similar pattern. Slight dissolution of hematite and kerogen-O also occurs. Kaolinite (Fig. 2b) dissolves steadily. K-feldspar and Na-smectite (Fig. 2b) and oligoclase (Fig. 2c) dissolve significantly until disappeared after about 50 ka. Illite (Fig. 2c) precipitates significantly throughout the simulation time. Carbonate mineral (Fig. 2d) calcite initially precipitates, and then dissolves steadily. Significant dawsonite and ankerite precipitation is obtained. Siderite initially precipitates, and then dissolves. Dolomite is not formed in this simulation. Changes of abundance of Quartz, albite-low and pyrite are not observed in the simulation.

For dunite, dissolution of forsterite and fayalite (Fig. 3) occurs at constant rates. As a result, magnesite and siderite precipitate due to the dissolution of the two primary reactant minerals and the CO_2 supply from injection. At the same time, talc and amorphous silica precipitation occurs. The simulation of olivine hydrolysis and the resultant formation of such secondary minerals is generally consistent with the serpentinization of ultra-mafic rocks. Ultra-mafic rocks usually contain other minor components, which are affected by the extremely reducing conditions induced by the hydrolysis

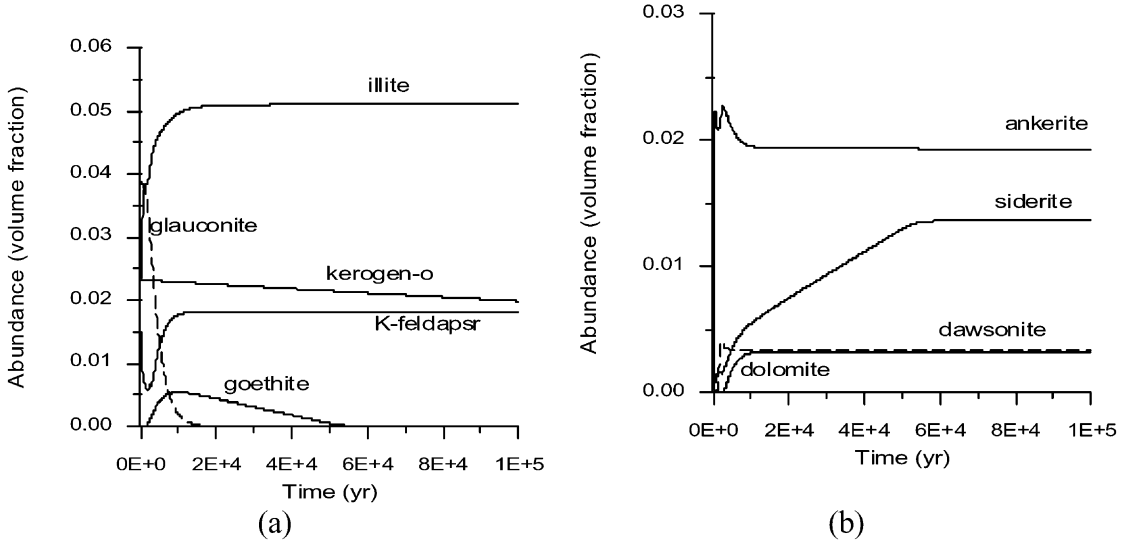

Fig. 1. Simulated mineral abundances after 100 ka in glauconitic sandstone with CO_2 injected at 260 bar.

of Fe(II). Because these components have been omitted, the application of natural analogues for validation would necessarily require more detailed simulations.

4.2. Capacity for CO_2 sequestration by minerals

For the glauconitic sandstone aquifer, the simulation suggests that a small amount of CO_2 is sequestered through precipitation of dolomite [$CaMg(CO_3)_2$] and dawsonite [$NaAlCO_3(OH)_2$]. A large amount of CO_2 is trapped by precipitation of siderite ($FeCO_3$) and ankerite [$(Mg,Ca,Fe(II))CO_3$]. The total amount of CO_2 trapped in mineral phases after 100 ka could reach about 17 kg per m^3 of medium (Fig. 4), which is greater than that dissolved in the aqueous phase (about 9 kg per m^3 of medium). The precipitation of siderite, either as a discrete carbonate or as a solid solution in more abundant Ca–Mg carbonates, or as ankerite [$(Mg,Ca,Fe(II))CO_3$], is conditioned by the redox state of the system. However, even relatively low partial pressures of H_2S would favor the fixation of Fe^{2+} as pyrite. This may decrease CO_2 sequestration in mineral phases.

For the Gulf Coast sediments, the CO_2 is immobilized by precipitation of 4 carbonate minerals: dawsonite, ankerite, calcite, and siderite. Most of the CO_2 is trapped by dawsonite and ankerite precipitation. After 100 ka, about 90 kg CO_2 per m^3 medium is trapped in the solid phase (Fig. 5). This may be the maximum amount

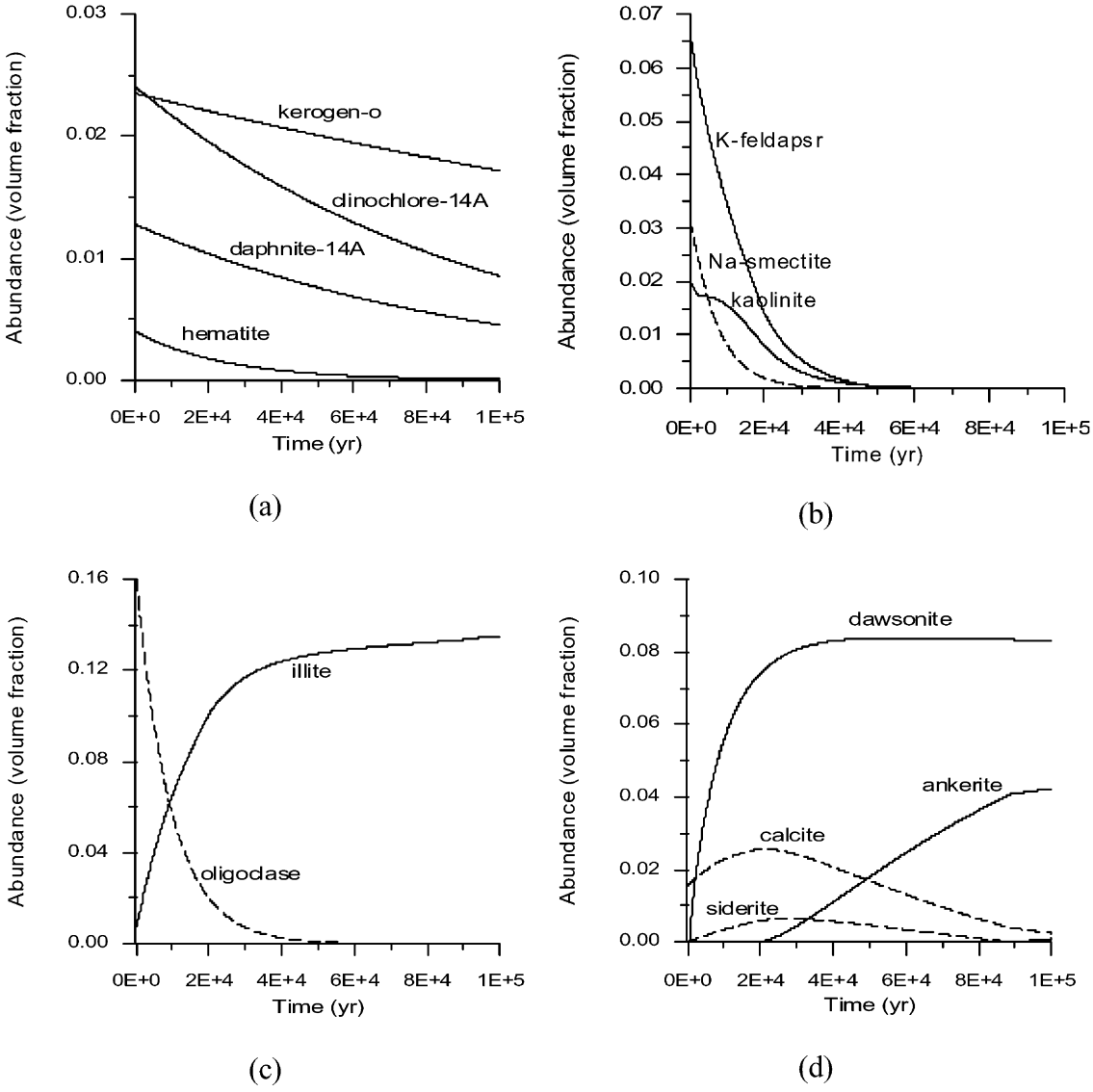

Fig. 2. Mineral abundances obtained during the interaction of groundwater with Gulf Coast sediments with CO_2 injected at 260 bar.

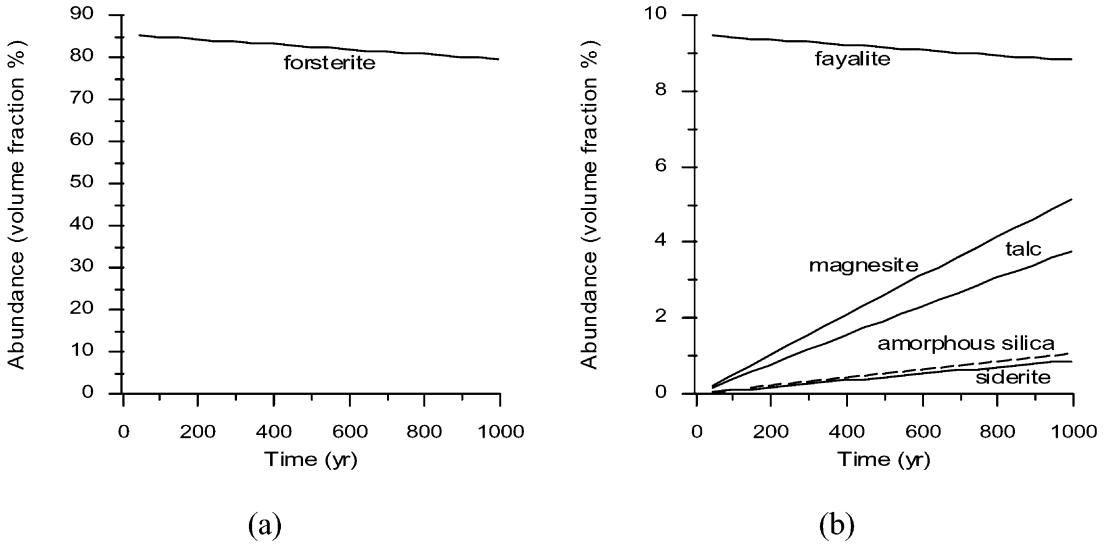

Fig. 3. Distribution of mineral phases obtained with CO_2 injection for the olivine rock.

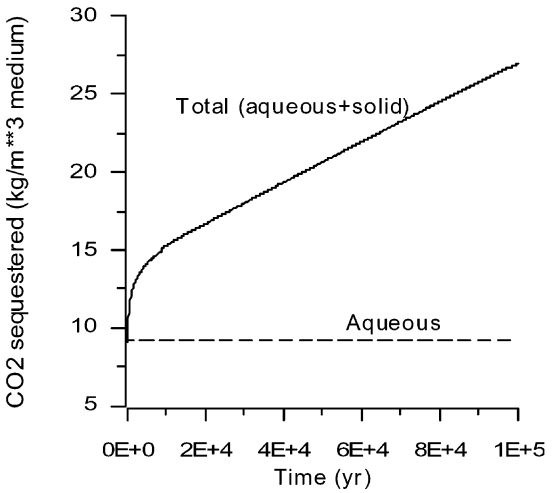

Fig. 4. Cumulative CO_2 sequestration in glauconitic sandstone with CO_2 injected at 260 bar.

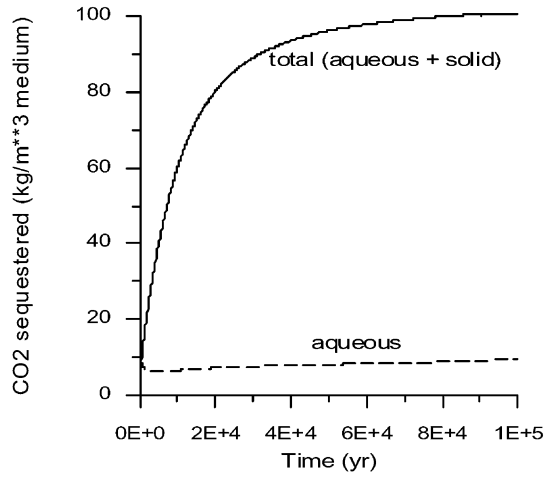

Fig. 5. Cumulative CO_2 sequestration obtained during the interaction of groundwater with Gulf Coast sediments with CO_2 injected at 260 bar.

for the current simulation because clinochlore-14A and daphnite-14A almost disappear (Fig. 2a). The capacity of CO_2 sequestration is proportional to abundance of these two minerals (source of Mg and Fe).

Dunite would have the largest capacity for CO_2 sequestration. One m^3 of medium could sequester as much as 100 kg CO_2 as secondary carbonate minerals (Fig. 6). However, sequestration of CO_2 in this rock type is considered impractical, not only because of its low crustal abundance, but also because of its limited porosity and the uncertain containment of CO_2 in dunitic rock masses.

4.3. Changes in porosity

All 3 examples demonstrate that rock alteration after CO_2 injection results in decreased porosity (Fig. 7). This is because CO_2 mass is added to the solid matrix due to mineral trapping. For dunite, the porosity after 1 ka has decreased to 0.6%. There is little free space to accommodate water and CO_2. The rock alteration and CO_2 sequestration processes would terminate when the porosity had declined to a negligible value.

A small decrease in porosity can result in a significant decrease in permeability. The decrease could reduce the

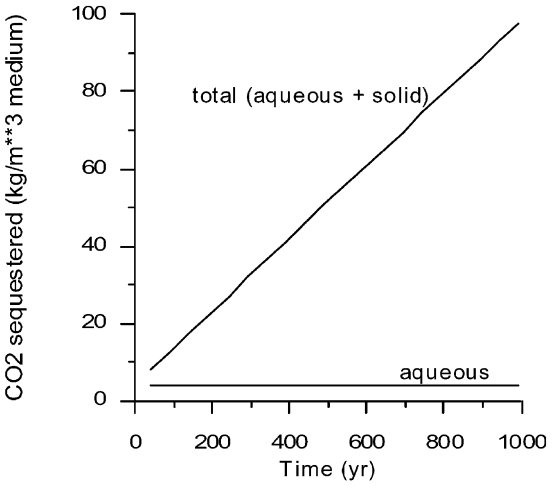

Fig. 6. Cumulative CO_2 sequestration for the olivine rock with CO_2 injected at 260 bar.

CO_2 injectivity. The changes in porosity are therefore a very important issue for CO_2 injection into deep geologic formations. Ross et al. (1982) observed a decreasing injectivity during CO_2 injection for enhanced oil recovery.

The alteration of ultramafic rocks under sub-critical hydrous conditions, while being simultaneously subjected to elevated CO_2 pressures, is a less likely natural scenario, although possible in actively subducting oceanic plate margins. An important feature of the alteration process is the substantial positive volume change of the solid phases upon alteration, due not only to the formation of a secondary hydrated phase, but also to the formation of magnesite and siderite. Volume expansion upon serpentinization of ultramafics has long been recognized in the literature, and implicit in this process is the elimination of residual porosity. The almost complete serpentinization of ultramafic rocks in ophiolitic assemblages suggests that the elimination of porosity is not of itself sufficient to prevent total serpentinization. The heavily fractured nature of serpentinites in the field, and multiple generations of sealed fractures, suggests that active tectonism may facilitate the process. Such conditions, however, would almost certainly disqualify any ultramafic rock as a potential CO_2 reservoir for safety reasons.

4.4. Sensitivity analysis to reaction rate

Sensitivity analyses with respect to reaction rate are based on the case of glauconitic sandstone. Two additional simulations were performed by respectively increasing and decreasing uniformly all surface areas listed in Table 2 by one order of magnitude. Scaling the surface areas for all minerals by the same factor is equivalent to scaling the time coordinate and does not lead to different results. Details on the sensitivity results are given elsewhere (Xu et al., 2000).

Because surface area scaling by the same constant factor may be inadequate, the effect of changing mineral surface areas relative to each another was also examined. Changes in the specific reactive surface area of any mineral by an increase or a decrease of one order of magnitude, except for glauconite do not affect either the dissolution of glauconite, or the precipitation of siderite and the amount of CO_2 sequestration. A decrease in the surface area for glauconite relative to other minerals causes a decrease in the dissolution rate of glauconite,

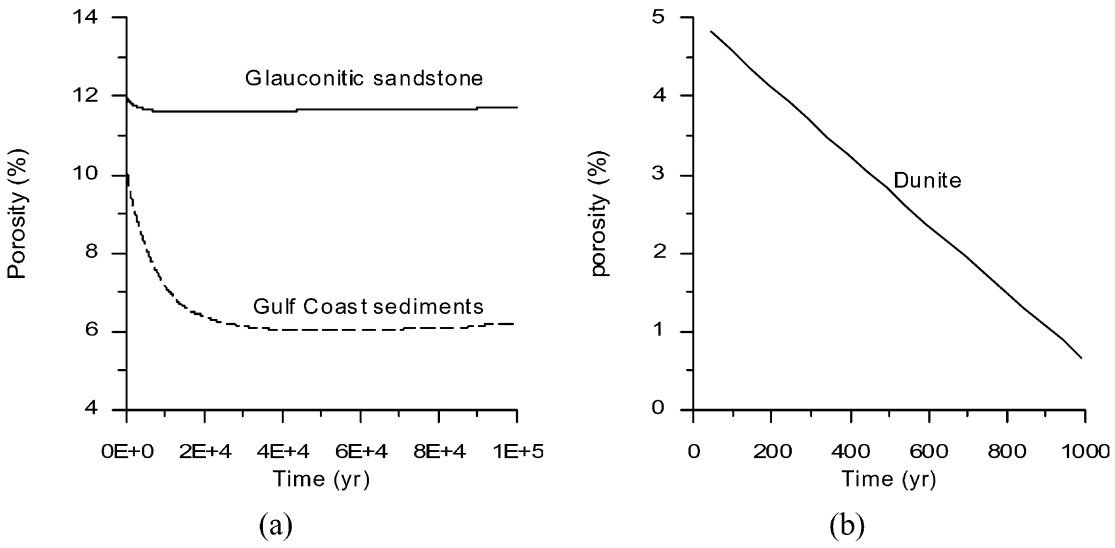

Fig. 7. Porosity evolution obtained from the three different rocks with CO_2 injected at 260 bar.

and thus a decrease in precipitation of siderite Consequently, the amount of CO_2 sequestration in mineral phases is less than the base case. An increase in the glauconite surface area has no effect on CO_2 sequestration. The dissolution of glauconite is redox sensitive. Glauconite dissolution involves a reduction of Fe^{3+} to Fe^{2+}. Therefore, the redox processes control the entire geochemical system. Further studies on the reduction of Fe^{3+} in glauconite may be very important for improved assessment of CO_2 disposal in this type of sediment.

5. Comparison of simulations with field observations

The confidence that can be placed on geochemical modeling of CO_2 sequestration is considerably enhanced if such modeling can be validated through comparison with field observations. Recently, mineralogical and groundwater chemical changes have been described in a lithic sandstone formation that has been invaded by magmatic CO_2 (Watson et al., 2002). The sandstone hosts the Ladbroke Grove gas field in South Australia, and can be compared with an adjacent gas reservoir with CO_2. Although the conditions differ somewhat from those of the Gulf Coast simulation given in this paper, a comparison is instructive. The similarities include the destruction of chlorite in the lithic fragments and net corrosion of the feldspars, a reduction in the concentration of calcite, an increase in the concentration of siderite and a significant increase in the quantity of ankerite. The most significant differences are the substantial increase in secondary kaolinite and no reported evidence of dawsonite formation even though an evaluation of the recovered groundwater indicates that it should have been supersaturated with respect to dawsonite. The porosity of the Ladbroke Grove reservoir also appears to have increased, whereas the present simulation shows a decrease. The simulation differs in that the CO_2 pressure is higher (260 vs. approximately 150 bar) and the Cl^- and Na^+ concentrations are somewhat higher.

Other field evidence supports that magmatic CO_2 can also lead to the formation of dawsonite in arenaceous sedimentary formations, notably in the Bowen, Gunnedah and Sydney Basins of New South Wales (Baker et al., 1995), and the Denison Trough of east-central Queensland (Baker, 1991; Baker and Caritat, 1992). Dawsonite and kaolinite in these sedimentary accumulations appear to have been produced at the expense of detrital feldspars, although it should be noted that feldspar destruction is incomplete, and on occasions, dawsonite is found in juxtaposition with unaltered feldspar (Loughnan and Goldbery, 1972). The field evidence is therefore suggestive of slow corrosion rates if not the eventual stabilization of feldspars. In these sedimentary formations, the occurrence of dawsonite formation is unrelated to the preceding precipitation or dissolution of diagenetic calcite, siderite and ankerite, which is attributed to early diagenesis and subsequent organic maturation (Baker, 1991).

Carbonate paragenesis in sedimentary formations invaded by magmatic CO_2 can vary in degree and complexity. The mineralogy, burial history, diagenesis, organic maturation, temperature and connate water salinity all play a role in addition to the timing and extent of magmatic CO_2 involvement. Thus it is hardly surprising that agreement between the present simulations and field observations is not perfect in all respects.

6. Limitation of simulations

Because of the chemical complexity of injection induced water–CO_2–rock interaction processes, an extensive theoretical framework is required to support the modeling of such systems. This framework is rarely if ever fully incorporated in geochemical models, nor are the algorithms used in geochemical codes always sufficient to meet the challenges involved. The range of problems for CO_2 in subsurface environments is far more extensive than any code presently accommodates. Because of numerous uncertainties and approximations, modeling currently cannot give a complete quantitative prediction of geochemical evolution of CO_2 injection. For example, the kinetics of heterogeneous reactions are scale and history-dependent, and cannot be reliably quantified. There is a lack of sufficiently detailed geochemical data at field sites. However, modeling is an excellent resource for analyzing and evaluating long-term CO_2 sequestration and geochemical performance. A critical evaluation of modeling results can provide useful insight into sequestration mechanisms and controlling geochemical conditions and parameters.

Several features of the simulations serve to highlight the need for a more critical evaluation both of the kinetic parameters required of the models, and of the role that organic matter and its decomposition play in the control of redox processes in the system. The complexities associated with quantitative prediction of heterogeneous processes need further elucidation and clarification if more realistic and quantifiable modeling is to be conducted successfully. While the current investigation indicates that the thermodynamic description of the current models demonstrate a semi-quantitative measure of the systems, the quantitative kinetic aspects are at best intelligent guesses.

In the model, the kerogen decarboxylation injects acetic acid (and acetate) into the brine. Aliphatic acids persist in oilfield brines and can exert a significant redox buffering effect (Helgeson et al., 1993). They also increase the solubility of metal species through complexation (Surdam et al., 1984), thus facilitating hetero-

geneous reactions and enhancing mass transport. Furthermore, oilfield brine data are suggestive that aliphatic acids are in metastable equilibrium with each other and with the HCO_3^- ion (Helgeson et al., 1993). The current model similarly assumes that equilibrium is maintained between acetic acid and the HCO_3^- ion through the redox reaction [Eq. (21)]. Homogeneous equilibrium with respect to CH_4 is also presumed in the model, thus:

$$CH4(aq) + 2O_2(g) = HCO_3^- + H^+ + H_2O \quad (22)$$

Subtracting Eq. (22) from Eq. (21), we get:

$$CH_3COOH(aq) + H_2O = HCO_3^- + H^+ + CH_4(aq) \quad (23)$$

This reaction has been investigated experimentally under a variety of conditions, and found to proceed extremely slowly in the aqueous phase, allowing acetic acid solutions to persist indefinitely (Kharaka et al., 1983; Bell and Palmer, 1994). However, the reaction can be catalyzed at the surfaces of some minerals, e.g. magnetite or Ca-smectite (Bell et al., 1994), leading to rates that are compatible with field observations regarding the formation of natural gas during diagenesis (Drummond and Palmer, 1986). Indeed, the formation of water soluble aliphatic acid precursors and their transport in pore waters is considered an essential step in the concentration of short chain alkanes in natural gas reservoirs (Carothers and Kharaka, 1978; Drummond and Palmer, 1986). Acetate concentrations observed in oil field brines are, however, incompatible with associated CH_4 partial pressures (Helgeson et al., 1993). Equilibrium between acetic acid and CH_4 is therefore not normally attained, and dispoportionation of acetic acid is slow in relation to its formation by decarboxylation of kerogen. The current model requires improvement by introducing reactions that place kinetic controls on the formation of CH_4 as represented either by the back reaction of Eq. (22), or by the acetic acid disproportionation reaction given by Eq. (23).

The processes by which oxygenated functional groups are lost from kerogen during diagenesis are not fully elucidated, although free radical mechanisms are probable (Eisma and Jurg, 1969; Weres et al., 1988). However, Xiao (2001) has shown that acid catalysed hydrolysis of ether and ester functional groups with the formation of secondary hydroxy groups in the presence of water is kinetically favored. Thus, the acidification of pore waters by high partial pressures of CO_2 could result in greatly accelerated decarboxylation of kerogen in adjacent shales. However, acid catalysed hydrolysis of water soluble esters to aliphatic acid and alcohol, dominates only at pHs lower than those expected during underground storage of CO_2 (Mabey and Mill, 1978).

Given that high partial pressures of CO_2 also increase the stability and concentration of acetic acid, total acetate concentrations in saline aquifers containing CO_2 at high pressures, would be likely to increase, especially if CH_4 formation were slow in relation to the enhanced decarboxylation rates. Should the total acetate concentration be significantly higher than predicted by the current model, acetate complexing with metal cations would also modify the solubility of some of the rock forming minerals including mineral trapping carbonates. Inclusion of acetate complexing in the model would therefore be warranted.

For large-scale injection of CO_2 into aquifers, geochemical processes are strongly affected by physical processes such as multiphase fluid flow, solute transport, and changes in effective stress. Fluid pressures will rise as CO_2 displaces aquifer water in which it partly dissolves. The dissolution of primary and precipitation of secondary minerals changes formation porosity and permeability, and then fluid flow patterns. The continuous injection of CO_2 will lead to increased formation pressures over large areas, of the order of 1000 km^2 or more (Pruess et al., 2001), which will modify the local mechanical stress field, causing deformation of the aquifer. All processes involving coupled hydrologic, mechanical and chemical effects influence the feasibility of CO_2 injection and storage in deep aquifers. No comprehensive coupled approaches have yet been used to analyze aquifer CO_2 disposal systems. Uncoupled batch geochemical modeling, flow simulations, and rock stress analyses are inadequate in describing the complex subsurface physical and chemical interactions expected to occur. A systematic process-based understanding of the coupled physical and chemical phenomena should be addressed in the future.

7. Summary and conclusions

Three host rock types have been evaluated for long-term CO_2 disposal in deep aquifers using a geochemical modeling tool (TOUGHREACT). Major conclusions that can be drawn are as follows:

1. CO_2 sequestration by mineral phases varies considerably with rock type. The capacity of a glauconitic sandstone aquifer (17 kg per m^3 of medium) is smallest among the 3. Gulf Coast sediments have a significant capacity (90 kg per m^3 of medium). Dunite has the largest sequestration capacity (100 kg per m^3 of medium). However, this rock type is not abundant in crustal rocks, and its fortuitous occurrence in a structural trap is unlikely. The trapping capacity depends significantly on mineral composition. For the glauconitic sandstone case, the capacity

is proportional to the abundance of glauconite. For the Gulf Coast sediments, it is proportional to the abundances of clinochlore-14A and daphnite-14A. The formation of CO_2-trapping mineral phases is case-dependent. For the glauconitic sandstone, most CO_2 is trapped as ankerite and siderite, with minor dolomite and dawsonite. For the Gulf Coast case, the major trapping minerals are dawsonite and ankerite, with minor calcite and siderite. For the olivine rock (dunite) case, the trapping minerals are magnesite and siderite. The mineral-trapping capacity can be comparable with or be larger than that of solubility trapping (7–10 kg per m^3 of medium).

2. The addition of CO_2 mass as secondary carbonates to the solid matrix results in decreased porosity. This in turn adversely affects permeability and fluid flow in the aquifer. Porosity decreases could reduce the CO_2 injectivity. Porosity degradation might be an important issue.
3. The time frame for CO_2 sequestration is a function of reaction kinetics. Sensitivity simulations show that scaling surface areas by the same constant factor is equivalent in scaling the time coordinate and otherwise does not lead to different results. The surface area changes lead to reciprocal changes in the time scale. Specific changes in the reactive surface area for redox sensitive minerals such as glauconite significantly affect mineral alteration and the extent of CO_2 sequestration.

The preliminary modeling presented in this paper shows considerable promise. Further improvement to the simulator is required, such as the incorporation of solid solution models, the kinetic control of homogeneous reactions in the aqueous phase such as acetate decomposition, and further refinement of all kinetic and thermodynamic parameters. Sensitivity studies are also merited. Furthermore, the current "black box" simulations cannot reveal complexities introduced by fluid phase transport. Thus reactive transport modeling must necessarily be used as a basis for comparison with field observations.

The range of problems concerning the interaction of water–CO_2–rock is very broad. The present simulation results are specific to the conditions and parameters considered. Care should be taken when extrapolating the results and conclusions for other sites. However, geochemical modeling is an excellent resource for analyzing and evaluating long-term CO_2 sequestration and geochemical performance. A critical evaluation of modeling results can provide useful insight into sequestration mechanisms and controlling geochemical conditions and parameters.

Acknowledgements

We are grateful to Ardyth Simmons and Nicolas Spycher for a review of the manuscript and suggestions for improvement. We acknowledge Yousif Kharaka and an anonymous reviewer for their detailed helpful suggestions and comments during the review process that significantly improved the quality of this paper. This work was supported by the Director, Office of Science, Office of Basic Energy Sciences, of the U.S. Department of Energy, under Contract No. DE-AC03-76SF00098 with Lawrence Berkeley National Laboratory.

References

Ague, J.J., Brimhall, G.H., 1989. Geochemical modeling of steady state and chemical reaction during supergene enrichment of porphyry copper deposits. Econ. Geol. 84, 506–528.

Arnorsson, S., Stefansson, A., 1999. Assessment of feldspar solubility constants in water in the range 0° to 350 °C at vapor saturation pressures. Am. J. Sci. 299, 173–209.

Apps, J.A., 1996. An approach to modeling of the chemistry of waste fluid disposal in deep saline aquifers. In: Apps, J.A., Tsang, C.F. (Eds.), Deep Injection Disposal of Hazardous and Industrial Waste: Scientific and Engineering Aspects. Academic Press, San Diego, California, pp. 465–488.

Bachu, S., Gunter, W.D., Perkins, E.H., 1994. Aquifer disposal of CO_2: hydrodynamic and mineral trapping. Energy Convers. Manag. 35, 269–279.

Bailey, S.W., 1986. AIPEA Newsletter Suppl. 22.

Baker, J.C., 1991. Diagenesis and reservoir quality of the Aldebaran Sandstone, Denison Trough, east-central Queensland, Australia. Sedimentol 38, 819–838.

Baker, J.C., Caritat, P., 1992. Postdepositional history of the Permian Sequence in the Denison Trough, Eastern Australia. Am. Assoc. Petrol. Geol. Bull. 76, 1224–1249.

Baker, J.C., Bai, G.P., Golding, S.D., Keene, J.B., 1995. Continental-scale magmatic carbon dioxide seepage recorded by dawsonite in the Bowen-Gunnedah-Sydney Basin system, Eastern Australia. J. Sed. Res. A65, 522–530.

Behar, F., Vandenbroucke, M., 1986. Representation chimique de la structure des kerogenes et des asphaltenes en fonction de leur origine et de leur degre d'evolution. Revue de L'Institut Francais du Petrole 41, 173–188.

Bell, J.L.S., Palmer, 1994. Experimental studies of organic acid decomposition. In: Pittman, E.D., Lewan, M.D. (Eds.), Organic Acids in Geological Processes, Chapter 9. Springer Verlag, Berlin, pp. 226–269.

Bell, J.L.S., Palmer, D.A., Barnes, H.L., Drummond, S.E., 1994. Thermal decomposition of acetate: III. Catalysis by mineral surfaces. Geochim. Cosmochim. Acta 58, 4155–4177.

Blum, A.E., Stillings, L.L., 1995. Feldspar dissolution kinetics, Chapter 7. In: White, A.F., Brantley, S.L. (Eds.), Chemical Weathering Rates of Silicate Minerals. Mineral Society of America 31, Washington DC, pp. 291–351.

Carothers, W.W., Kharaka, Y.K., 1978. Aliphatic acid anions in oil-field waters—implications for origin of natural gas. Am. Assoc. Petrol. Geol. Bull. 62, 2441–2453.

Chai, L., Navrotsky, A., 1996. Synthesis, characterization, and energetics of solid solution along the dolomite-ankerite join, and implications for the stability of ordered CaFe(CO3)2. Am. Mineral. 81, 1141–1147.

Chermak, J.A., Rimstidt, J.D., 1989. Estimating the thermodynamic properties ($\Delta G^o f$ and $\Delta H^o f$) of silicate minerals at 298 K from the sum of polyhedral contributions. Am. Mineral. 74, 1023–1031.

Drummond, J.M., Jr., 1981. Boiling and mixing of hydrothermal fluids: Chemical effects on mineral precipitation, Ph.D. thesis, Pennsylvania State Univ.

Drummond, S.E., Palmer, D.A., 1986. Thermal decarboxylation of acetate. Part II. Boundary conditions for the role of acetate in the primary migration of natural gas and the transportation of metals in hydrothermal systems. Geochim. Cosmochim. Acta 50, 813–823.

Eisma, E., Jurg, J.W., 1969. Fundamental aspects of the generation of petroleum. Chapter 28. In: Eglinton, G., Murphy, M.T.J. (Eds.), Organic Geochemistry: Methods and Results. Springer-Verlag, New York.

Essene, E.J., 1983. Solid solutions and solvi among metamorphic carbonates with applications to geologic thermobarometry. In: Reeder, R.J. (Ed.), Carbonates: Mineralogy and Chemistry, Reviews in Mineralogy, 11, Chapter 2. Mineralogical Society of America, pp. 49–76.

Ferrante, M.J., Stuve, J.M., Richardson, D.W., 1976. Thermodynamic data for synthetic dawsonite. US Bureau of Mines Report of Investigations No. 8129.

Folk, R.L., 1968. Petrology of Sedimentary Rocks. Hemphill Publishing Company, Austin, Texas.

Franks, S.G., Forester, R.W., 1984. Relationships among secondary porosity, pore fluid chemistry and carbon dioxide, Texas Gulf Coast. In: McDonald, D.A., Surdam, R.C. (Eds.), Clastic Diagenesis. AAPG Memoir 37, Part 1, Concepts and Principles, pp. 63–78.

Goldsmith, R., 1983. Phase relations of rhombohedral carbonates. In: Reeder, R.J. (Ed.), Carbonates: Mineralogy and Chemistry, Reviews in Mineralogy, 11, Chapter 2. Mineralogical Society of America, pp. 49–76.

Gouze, P., Coudrain-Ribstein, A., 2002. Chemical and porosity changes during sedimentary diagenesis. Appl. Geochem. 17, 39–47.

Gunter, W.D., Bachu, S., Law, D.H.S., Marwaha, V., Drysdale, D.L., MacDonald, D.E., McCann, T.J., 1996. Technical and economic feasibility of CO_2 disposal in aquifers within the Alberta Sedimentary Basin, Canada. Energy Convers. Manag. 37, 1135–1142.

Gunter, W.D., Perkins, E.H., McCann, T.J., 1993. Aquifer disposal of CO_2-rich gases: reaction design for added capacity. Energy Convers. Manag. 34, 941–948.

Gunter, W.D., Wiwchar, B., Perkins, E.H., 1997. Aquifer disposal of CO_2-rich greenhouse gases: extension of the time scale of experiment for CO_2-sequestering reactions by geochemical modeling. Mineral. Petrol. 59, 121–140.

Helgeson, H.C., Kirkham, D.H., 1974. Theoretical prediction of the thermodynamic behaviour of aqueous electrolytes at high pressures and temperatures: II. Debye-Hückel parameters for activity coefficients and relative partial molal properties. Am. J. Sci. 274, 1199–1261.

Helgeson, H.C., Delany, J.M., Nesbitt, H.W., Bird, D.K., 1978. Summary and critique of the thermodynamic properties of rock-forming minerals. Am. J. Sci. 278A, 1–229.

Helgeson, H.C., Knox, A.M., Owens, C.E., Shock, E.L., 1993. Petroleum, oil field waters, and authigenic mineral assemblages. Are they in metastable equilibrium in hydrocarbon reservoirs? Geochim. Cosmochim. Acta 57, 3295–3339.

Helgeson, H.C., Owens, C.E., Knox, A.M., Richard, L., 1998. Calculation of the standard molal thermodynamic properties of crystalline, liquid, and gas organic molecules at high temperatures and pressures. Geochim. Cosmochim. Acta 62, 985–1081.

Hitchon, B. (Ed.), 1996. Aquifer Disposal of Carbon Dioxide. Geoscience Publishing, Ltd, Sherwood Park, Alberta, Canada.

Holland, T.J.B., Powell, R., 1998. An internally consistent thermodynamic data set for phases of petrological interest. J. Metamorph. Geol. 16, 309–343.

Holloway, S., 1997. An overview of the underground disposal of carbon dioxide. Energy Convers. Manag. 38, 193–198.

Hunt, J.M., 1972. Distribution of carbon in the earth's crust. Bull. Am. Assoc. Petrol. Geol. 56, 2273–2277.

Johnson. J.W., Nitao, J.J., Steefel, C.I., Knaus, K.G., 2001. Reactive transport modeling of geologic CO_2 sequestration in saline aquifers: the influence of intra-aquifer shales and the relative effectiveness of structural, solubility, and mineral trapping during prograde and retrograde sequestration, In Proc.: 1st Nat. Conf. Carbon Sequestration. Washington, DC.

Johnson, J.W., Oelkers, E.H., Helgeson, H.C., 1992. SUPCRT92: a software package for calculating the standard molal thermodynamic properties of minerals, gases, aqueous species, and reactions from 1 to 5000 bars and 0 to 1000 degrees C. Comput. Geosci. 18, 899–947.

Kharaka, Y.K., Carothers, W.W., Rosenbauer, R.J., 1983. Thermal decarboxylation of acetic acid, implications for origin of natural gas. Geochim. Cosmochim. Acta 47, 397–402.

Knauss, K.G., Wolery, T.J., 1989. Muscovite dissolution kinetics as a function of pH and time at 70 °C. Geochim. Cosmochim. Acta 53, 1493–1501.

Koster, H.M., 1982. The crystal structure of 2:1 layer silicates. In: Van Olphen, H., Veniale, F. (Eds.), Developments in Sedimentology, vol. 35. Elsevier, Scientific Publishing Co, New York, pp. 41–71.

Korbol, R., Kaddour, A., 1995. Sleipner vest CO_2 disposal - injection of removed CO_2 into the Utsira Formation. Energy Convers. Manag. 36, 509–512.

Kulik, D.A., Aja, S.U., 1997. Hydrothermal stability of illite: implications of empirical correlations and Gibbs Energy minimization. Proc. 5th Internat. Symp. Hydrothermal Reactions, Gatlinburg, Tennessee, pp. 228–292.

Land, L.S., 1984. Frio sandstone diagenesis, Texas Gulf Coast: a regional isotopic study. In: McDonald, David A., Surdam, Ronald C. (Eds.), Clastic Diagenesis. AAG Memoir 37, Part 1. Concepts and Principles, pp. 47–62.

Lasaga, A.C., 1984. Chemical kinetics of water-rock interactions. J. Geophys. Res. 89, 4009–4025.

Law, D.H.S., Bachu, S., 1996. Hydrogeological and numerical analysis of CO_2 disposal in deep aquifers in the Alberta Sedimentary Basin. Energy Convers. Manag. 37, 1167–1174.

Lohuis, J.A.O., 1993. Carbon dioxide disposal and sustainable development in The Netherlands. Energy Convers. Manag. 34, 815–821.

Loucks, R.G., Dodge, M.M., Galloway, W.E., 1984. Regional controls on diagenesis and reservoir quality in Lower Tertiary sandstones along the Texas Gulf Coast. In: McDonald, D.A., Surdam, R.C. (Eds.), Clastic Diagenesis. AAG Memoir 37, Part 1. Concepts and Principles, pp. 15–45.

Loughnan, F.C., Goldbery, R., 1972. Dawsonite and analcite in the singleton coal measures of the Sydney Basin. Am. Mineral. 57, 1437–1447.

Mabey, W., Mill, T., 1978. Critical review of hydrolysis of organic compounds in water under environmental conditions. J. Phys. Chem. Ref. Data 7, 383–415.

McPherson, B.J.O.L., Lichtner, P.C., 2001. CO_2 sequestration in deep aquifers, In Proceedings: 1st Nat. Conf. Carbon Sequestration. Washington, DC.

Nagy, K.L., 1995. Dissolution and precipitation kinetics of sheet silicates. Chem. Weath. Rates Silicate Minerals 31, 291–351.

Narasimhan, T.N., Witherspoon, P.A., 1976. An integrated finite difference method for analyzing fluid flow in porous media. Water Resour. Res. 12, 57–64.

Newton, R.C., Charlu, T.V., Kleppa, O.J., 1980. Thermochemistry of the high structural state plagioclases. Geochim. Cosmochim. Acta 44, 933–942.

Nordstrom, D.K., Muñoz, J.L. (Eds.), 1986. Geochemical Thermodynamics. The Benjamin/Cummings Pub. Co, Menlo Park, California.

Ortoleva, P.J., Dove, P., Richter, F., 1998. Geochemical perspectives on CO_2 sequestration, Manuscript prepared for US Department of Energy Workshop on "Terrestrial Sequestration of CO_2—An Assessment of Research Needs," Gaithersburg, MD.

Parkhurst, D.L., Thorstenson, D.C., Plummer, L.N., 1980. PHREEQE: a computer program for geochemical calculations. US Geol. Surv., Water Resour. Investig. 80–96.

Pearce, J.M., Holloway, S., Wacker, H., Nelis, M.K., Rochelle, C., Bateman, K., 1996. Natural occurrences as analogues for the geological disposal of carbon dioxide. Energy Convers. Manag. 37, 1123–1128.

Perkins, E.H., Gunter, W.D., 1995. A users manual for PATHARC.94: a reaction path-mass transfer program, Alberta Research Council Report ENVTR 95-11, Canada.

Pruess, K., 1991. TOUGH2: A General Numerical Simulator for Multiphase Fluid and Heat Flow, Lawrence Berkeley Laboratory Report LBL-29400, Berkeley, California.

Pruess, K., Xu, T., Apps, J., García, J., 2001, Numerical Modeling of Aquifer Disposal of CO2, Paper SPE-66537, presented at SPE/EPA/DOE Exploration and Production Environmental Conference, San Antonio, TX, USA.

Reed, M.H., 1982. Calculation of multicomponent chemical equilibria and reaction processes in systems involving minerals, gases and aqueous phase. Geochim. Cosmochim. Acta 46, 513–528.

Richard, L., Helgeson, H.C., 1998. Calculation of the thermodynamic properties at elevated temperatures and pressures of saturated and aromatic high molecular weight and liquid hydrocarbons in kerogen, bitumen, petroleum and other organic matter of biogeochemical interest. Geochim. Cosmochim. Acta 62, 3591–3636.

Rimstidt, J.D., 1997. Quartz solubility at low temperatures. Geochim. Cosmochim. Acta 61, 2553–2558.

Rochelle, C.A., Bateman, K., Pearce, J.M., 1996. Fluid-rock interactions resulting from the underground disposal of carbon dioxide, In Bottrell, S. H. (ed.), Proc., 4th Internat. Symp. Geochemistry of the Earth's Surface. University of Leeds, Dept. of Earth Sciences, Leeds, UK., pp. 448–452.

Ross, G.D., Todd, A.C., Tweedie J.A., Will, A.G.S., 1982. The dissolution effects of CO_2-brine systems on the permeability of U.K. and North Sea Calcareous Sandstones. Society of Petroleum Engineers/U.S. Department of Energy 3rd Joint Symp. Enhanced Oil Recovery, Paper SPE/DOE 10685, pp. 149–154.

Shock, E.L., Sassani, D.C., Willis, M., Sverjensky, D.A., 1997. Inorganic species in geologic fluids, Correlations among standard molal thermodynamic properties of aqueous ions and hydroxide complexes. Geochim. Cosmochim. Acta 61, 907–950.

Sonnenthal, E.L., Spycher, N., 2001. Drift-Scale coupled processes (DST and THC seepage) models. AMR N0120/U0110 Rev.01, Yucca Mountain Project. Lawrence Berkeley National Laboratory, Berkeley, California.

Spycher, N.F., Reed, M.H., 1988. Fugacity coefficients of H_2, CO_2, CH_4, H_2O and of H_2O-CO_2-CH_4 mixtures: a virial equation treatment for moderate pressures and temperatures applicable to calculations of hydrothermal boiling. Geochim. Cosmochim. Acta 52, 739–749.

Surdam, R.C., Boese, S.W., Crossey, L.J., 1984. The chemistry of secondary porosity. AAPG Memoir 37 (Clastic Diagenesis), 317–345.

Svensson, U., Dreybrodt, W., 1992. Dissolution kinetics of natural calcite minerals in CO_2-water systems approaching calcite equilibrium. Chem. Geol. 100, 129–145.

Steefel, C.I., Lasaga, A.C., 1994. A coupled model for transport of multiple chemical species and kinetic precipitation/dissolution reactions with applications to reactive flow in single phase hydrothermal system. Am. J. Sci. 294, 529–592.

Steefel, C.I., van Cappellen, P., 1990. A new kinetic approach to modeling water-rock interaction: the role of nucleation, precursors and Ostwald ripening. Geochim. Cosmochim. Acta 54, 2657–2677.

Stumm, W., Morgan, J.J., 1981. Aquatic Chemistry: An Introduction Emphasizing Chemical Equilibria in Natural Waters. John Wiley & Sons, New York.

Tempel, R.N., Harrison, W.J., 2000. Simulation of burial diagenesis in the Eocene Wilcox Group of the Gulf of Mexico basin. Appl. Geochem. 15, 1071–1083.

Tester, J.W., Worley, G.W., Robinson, B.A., Grigsby, C.O., Feerer, J.L., 1994. Correlating quartz dissolution kinetics in pure water from 25° to 625 °C. Geochim. Cosmochim. Acta 58, 2407–2420.

Watson, M.N., Zwingmann, N., Lemon, N.M., 2002. The Ladbroke Grove-Katnook carbon dioxide natural laboratory: A recent CO2 accumulation in a lithic sandstone reservoir. Extended Abstract E1-5, 6th Internat. Conf. Greenhouse Gas Control Technologies (GHCT-6), Kyoto, Japan.

Weres, O., Newton, A.S., Tsao, L., 1988. Hydrous pyrolysis of alkanes, alkenes, alcohols and ethers. Org. Geochem. 13, 433–444.

White, S.P., Weir, G.J., Kissling, W.M., 2001. Numerical simulation of CO_2 sequestration in natural CO_2 reservoirs on the Colorado Plateau. In Proc. 1st Nat. Conf. Carbon Sequestration, Washington, DC.

Wolery, T.J., 1992. EQ3/6: Software package for geochemical modeling of aqueous systems: Package overview and installation guide (version 7.0). Lawrence Livermore National Laboratory Report UCRL-MA-110662 PT I, Livermore, California.

Xiao, Y., 2001. Modeling the kinetics and mechanisms of petroleum and natuaral gas generation: a first principles approach. Chapter 11 in Molecular Modeling, (Eds.) Reviews in Mineralogy and Geochemistry, Mineralogical Society of America, Washington, D.C., 42, pp. 383–436.

Xu, T., Pruess, K., 1998. Coupled modeling of non-isothermal multiphase flow, solute transport and reactive chemistry in porous and fractured media: 1. Model development and validation. Lawrence Berkeley National Laboratory Report LBNL-42050, Berkeley, California.

Xu, T., Pruess, K., 2001. On fluid flow and mineral alteration in fractured caprock of magmatic hydrothermal systems. J. Geophys. Res. 106, 2121–2138.

Xu, T., Apps, J., Pruess, K., 2000. Analysis of mineral trapping for CO_2 disposal in deep aquifers, Lawrence Berkeley National Laboratory Report LBNL-46992, Berkeley, California.

Yeh, G.T., Tripathi, V.S., 1991. A model for simulating transport of reactive multispecies components: model development and demonstration. Water Resour. Res. 27, 3075–3094.